Haptic Surgical Simulation: An Application to Virtual Suture

Lian L. L. and Chen Y. H.

The University of Hong Kong, lianlili@hkusua.hku.hk, yhchen@hkucc.hku.hk

ABSTRACT

Virtual surgical planning and training require high fidelity not only in visual modeling, but also in haptic modeling. As a fundamental and typical application of surgical simulation, virtual suturing deals with technical problems such as soft tissue modeling, collision detection, and force modeling. In this paper, a haptic system of virtual suture is developed for surgical training. A realistic tissue modeling method based on either MRI or CT images is proposed. Given a CT or MRI file, an STL file is constructed. The STL file is voxelized to generate a regular spatial lattice that provides the basis for constructing the mass-spring system (MSS). Surface textures are mapped to this MSS for better visual effect of human tissues. Haptic interaction between the tissue model and a haptic device is rendered on a piecewise linear stress-strain model. A prototype system based on the proposed method is implemented. When using this system, a user can feel the force change at different stage of the suturing process. A force bar recording and showing the changing force in the suturing process provides an intuitive way of force magnitude display.

Keywords: haptics, surgical simulation, suture, deformable object.

1. INTRODUCTION

With the rapid development of computer power, graphics capabilities, and haptic hardware technologies, there is a growing interest to apply virtual reality and simulation techniques into surgical planning and training systems. Various virtual simulation systems concerning tissue deformation, tool interaction, visual rendering, and force feedback have been reported in recent years. Christian et al. set up a surgery training system which realized collision detection, haptic interaction and topology modification based on the long element method [4]. Stephane et al. proposed a hybrid model based on linear elasticity theory and finite-element modeling that is well suited for surgery simulation [22]. Kuhnapfel et al. developed a virtual reality training system for minimally invasive surgery which can create a surgical scene containing deformable organ models quickly [13]. Picinbono et al. developed a minimally invasive hepatic surgery simulator prototype [20]. They improved the overall realism of the system by using force extrapolation algorithm and creating biomechanical models that include anisotropic deformation. Kim et al. presented a novel approach to rapid collision detection and a new meshless numerical scheme to achieve a trade-off between realism and computation speed [12]. In [5], Bielser et al. presented a framework for interactive simulation of surgical cuts. They based the framework on tetrahedral volume meshes to achieve more topological flexibility. A mechanical scalpel model for haptic rendering and force feedback in surgical operation is illustrated.

As a typical and fundamental application of surgical training, suture simulation deals with techniques such as soft tissue modeling, haptic rendering, collision detection, etc. It has been reported by some researchers [1][11][13] in recent years. Almost all of these researches reported only conceptual ideas with no detailed description of all the technical problems encountered during the suture simulation partly because techniques for the simulation were pre-mature at that time. Even though the technologies have seen great improvement today, development of a realistic surgical simulation remains a great challenge that has attracted many researchers worldwide.

Soft tissue modeling and haptic rendering are the most important problems in surgery simulation. Mass-spring system (MSS) and finite element method (FEM) are two major commonly used models for representing deformable objects. FEM is based on continuum mechanics. The continuous feature of this model makes it more realistic in simulations at the cost of being less efficient, so it is often used in static simulations. Recently, great effort has been made to apply FEM in real time simulation. Weiss et al. modeled skeletal muscle using the FEM method [8]. By applying non-linear forces to the model nodes, they verified the hypothesis that human and animal figures could be accurately generated

by simulating the muscle action and resulting forces propelling the figure. Morten and Stephane developed a surgery simulation system using the finite element method [16]. They proposed to use approaches of linear elastic deformation and condensation to achieve real-time performance. Morten developed a simulation system to utilize three dimensional solid finite element models based on linear elasticity [17]. Real time performance was achieved by the use of pre-computation of the boundary conditions governing tissue behaviors. Berkley presented a new real-time methodology based on linear FE analysis [10]. This methodology is characterized by high model resolution, low preprocessing time, unrestricted multipoint surface contact, and adjustable boundary conditions.

Compared with FEM, MSS is more suitable for haptic simulation of large deformation due to its higher computing speed, theoretical correctness in large deformation, and topology change supporting. MSS is made up of mass points and massless springs connecting each mass point. Its dynamics can be well and easily understood, but it failed to simulate the deformable objects very accurately and concisely. Much work has been done to raise the realism of the model. In [6], Hutchinson et al. made refinement to the portion of object modified during the simulation to produce more realistic results and reduce the computation cost. Nedel and Thaimann added angular springs to conventional MSS to control the muscle volume during the simulation [18]. Bourguignon and Cani added volume force for both tetrahedral and hexahedral MSS. In addition to constant volume deformation, the resulting model achieved the ability of anisotropic control [2]. Diego et al. made use of two-layer MSS that includes both linear and non-linear springs to simulate the deformation of human thigh [5]. In [7], Weiss and Okamura developed a haptic tissue cutting system by creating two 2-dimensional deformable mass-spring-damper meshes: the larger one is used to calculate translational forces, the smaller one is used to calculate cutting forces. In this way, the smaller mesh can be assigned higher resolution so as to get higher realism.

In this research, the MSS approach is used because it is easier to meet the 1kHz update rate requirement of the haptic device PHANToM® used in the system. It is also easier to support the topology change during the suturing process. The paper is organized into 4 sections. The method used to determine the physical parameters of a soft tissue model, specifically, the stiffness coefficient of the connecting springs is discussed in section 2. Detailed procedure of the suturing process rendering is discussed in section 3, and conclusions are drawn in section 4.

2. SOFT TISSUE MODELING

The geometry of soft tissue is represented by the multi-layer structure as shown in Fig.1. It is a regular lattice structure at rest state. In the figure, each point represents a mass element, and each line represents a damping spring connecting two mass elements. Diagonal springs are added so that the soft tissue representation could resist shear stress. Because mass-spring systems have been widely applied in soft tissue modeling in surgical simulations, basic ideas will not be elaborated here. Instead, the method of determining the stiffness coefficient of the springs will be covered.

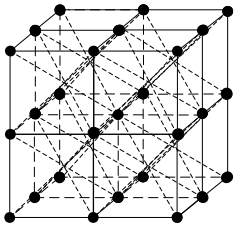

Fig. 1. A multi-layer lattice structure.

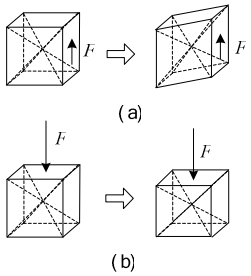

Fig. 2. Deformation of a voxel.

2.1 Determination of the Stiffness Coefficient

Stiffness of connecting springs is determined by the Young's modulus of the model simulated. When pure shear force F_s is exerted to one single voxel of the MSS (Fig.2(a)), it can be calculated according to the shear angle and the stiffness of the diagonal spring,

$$F_s = 2k_d \cdot a \cdot (2\tan\gamma - \sqrt{3} \cdot \frac{1+\tan\gamma}{\sqrt{2+(1+\tan\gamma)^2}} + \sqrt{3}\frac{1-\tan\gamma}{\sqrt{2+(1-\tan\gamma)^2}}) \quad (1)$$

where k_d is the stiffness of the diagonal spring, r is the shear angle, a is the original length of the normal spring. From the theory of solid mechanics, when the deformation is small, the shear stress can be calculated in Eqn.(2),

$$\tau = G \cdot \gamma \tag{2}$$

where τ is the shear stress, G is the shear modulus, and r is the shear angle. and also,

$$\tau = \frac{F_s}{a^2} \tag{3}$$

From Eqn.(1) to Eqn.(3), Eqn.(4) can be obtained,

$$k_d = \frac{Ga}{2} \cdot f(\gamma), \quad f(\gamma) = \gamma \cdot (2\tan\gamma - \sqrt{3} \cdot \frac{1+\tan\gamma}{\sqrt{2+(1+\tan\gamma)^2}} + \sqrt{3}\frac{1-\tan\gamma}{\sqrt{2+(1-\tan\gamma)^2}})^{-1} \tag{4}$$

The average of *f(r)* when *r* varies from 0 to 0.5 in radian is 1.5, using the average to replace *f(r)* in Eqn.(5), k_d can be formulated as,

$$k_d = 0.75Ga \tag{5}$$

For incompressible materials,

$$k_d = 0.25Ea$$

where E is the Young's modulus of the material. Similarly, when the normal force is exerted to the voxel (Fig.2(b)), stiffness of normal springs can be formulated as Eqn.(6). Details are omitted here because of the page limit.

$k_n = 0.45Ea$

2.2 Nonlinear Properties of the Soft Tissue

Soft tissues always show nonlinear, viscoelastic, and anisotropic properties. Experimental results of the stress-strain curve of muscle and skin are given in [15] [25]. To simulate the nonlinear relationship between stress and strain, piecewise linear functions are used to approximate the stress-strain curve. For the skin, it can be identified that when the deformation is less than 30 percent or larger than 60 percent, the stress-strain curve is almost linear [15], so three segmentations are made (as shown in Fig. 3(a)); whereas for the muscle, more segmentations have to be used (Fig. 3(b)).

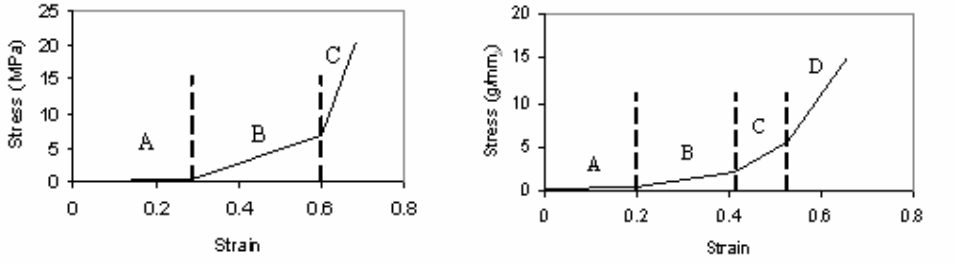

(a) Skin (b) Muscle

Fig. 3. Piecewise stress-strain curve for the simulation.

2.3 Geometry Data Acquisition and Haptic Model Construction

Fig. 4 is the flowchart illustrating how the MSS is constructed using CT or MRI scanning data. By CT or MRI scanning of human tissue, data files that contain gray value of voxels are obtained. With the aid of the commercial software 3D-doctor®, segmentations of voxels are made and different tissues are identified. Then each kind of tissue is reconstructed into a 3D surface model (STL file format). To construct the regular lattice structure of the MSS, 3D surface models are voxelized and points on the outer surface are extracted. These extracted points serve as mass elements of the MSS.

In this research, CT files of a human hand are used. Three kinds of tissues, skin, muscle, and bone are segmented (as pointed out in Fig. 5(a)) and STL files are generated for each kind of the tissue. Fig. 5 (b) shows a clearer image of the bone. Fig. 6 shows the result of muscle voxelization. To focus the description on the suturing operation, only a small

portion of the hand as highlighted by the dashed is used for MSS construction. Fig. 7 shows the detached MSS and the gap in the middle is generated manually to represent a wound.

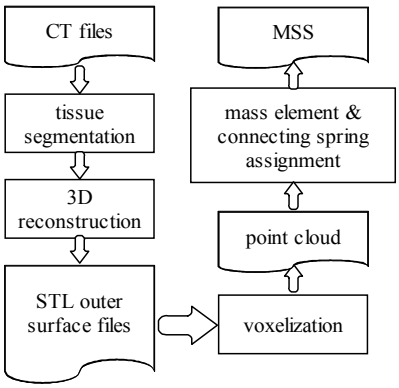

Fig. 4. Flowchart of data acquisition.

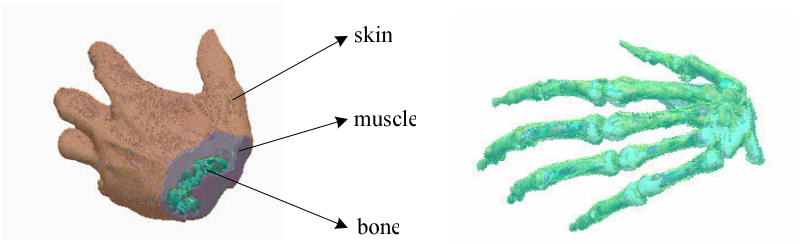

(a) (b)

Fig. 5. 3D reconstruction.

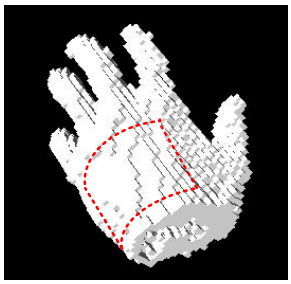

Fig. 6 Voxelization of tissue.

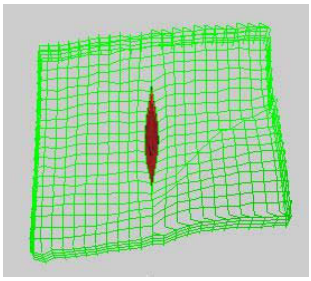

Fig. 7. The detached MSS with a wound.

3. SIMULATION OF SUTURING

3.1 Needle Insertion and Needle Motion Constraints

The force model during needle insertion into soft tissue is dependent on several factors such as the type of the tissue, the diameter of the needle and so on. The relationship between needle displacement and applied force is nonlinear [19] [21]. Here, the force model adapted from [21] as shown in Fig. 8 is used to simulate the force feedback during the process of needle insertion. Fig. 9(a) shows the MSS model in Fig. 7 with texture mapping. Fig.9(b) shows deformation of the tissue when the needle tries to penetrate in. When inserting the needle, the force feedback increases with the increase of the deformation until it reaches the force threshold (F_0 in Fig. 8), and the needle penetrates into the tissue. In real suturing, the needle is inserted into the tissue, then it penetrates through the tissue, and finally is pulled out of the tissue (Fig. 10 (a)) [24]. This process is simplified by regarding the entry point (point *A* is Fig. 10 (b)) overlap with the exit point (point *B* in Fig. 10 (b)). However, to achieve a more realistic force feedback, once the needle penetrates into the tissue, five degrees of freedom (DOF) of the needle are constrained.

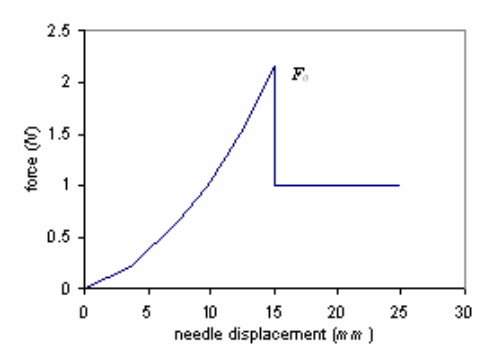

Fig. 8. Force model for needle insertion.

(a) before needle insertion (b) tissue deformation during the insertion

Fig. 9. Tissue deformation during needle insertion.

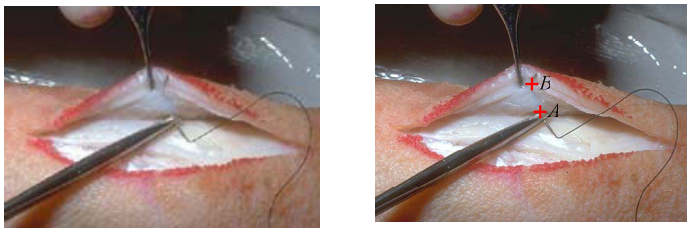

(a) (b)

Fig. 10. Real suturing.

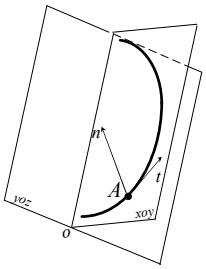

Fig. 11. Degree of freedom of the needle.

Fig. 12. Movement of the needle under the constraint.

As shown in Fig. 11, the needle is represented by a semicircle and it defines a plane named *xoy*. *A* is the constraint point, *t* is at the tangent to the circle and *n* is the normal of the circle at point A. When the needle penetrates into the tissue, only translation along direction *t* is allowed under the constraint of point *A*. Fig. 12 illustrates the movement of the needle under the constraints.

3.2 Suture Simulation

Because the suture is made up of materials of low elasticity, Brown modeled the suture as articulated object which was made up of linear links connected by spherical joints [11]. To simplify the calculation, in this research, the suture is modeled as mass-spring system of high stiffness as shown in Fig.13. In the figure, filled spheres N_0 to N_{n-1} represent the mass elements, and lines between each pair of spheres represent the connecting springs. Motion of the suture is firstly constrained by the movement of the needle. As shown in the figure, displacement of mass element N_0, the head of the suture, is fully constrained by the needle; and displacement of mass element N_{n-1}, the tail of the suture, is constrained by the sutured tissue. Other interactions acted on the suture include the gravity (Fig. 14) and the collision with the soft tissue. So the dynamic equation for each mass element can be expressed as,

$$m_i\ddot{x}_i + c_i\dot{x}_i + \sum F_i = \sum P_i \tag{7}$$

where m_i, c_i, x_i and F_i represent the mass, damping coefficient, displacement, and the spring force of element i, P_i represents the external force acted on element i, it includes the gravity G and the collision force P_c.

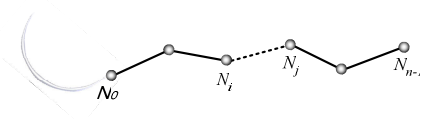

Fig. 13. Model of the suture.

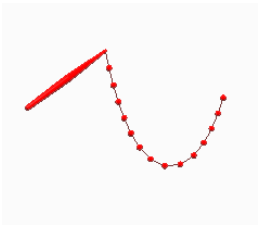

Fig. 14. A suture under the effect of gravity.

3.3 Collision Response of Suture

Collision detection between deformable objects is complicated and time consuming [3] [9] [14]. In this research, collisions between the series of mass elements as shown in Fig. 14 that make up the suture and the outer surface of the tissue model are checked. When a mass element of the suture collides with the outer surface of the tissue, a responsive force will be exerted to the element based on the "penalty method". As shown in Fig. 15, when the mass element N_i collides with the outer surface, penalty force P_c, which is calculated in Eqn.(8), will be exerted to element N_i,

$$Pc = k \cdot \Delta x \tag{8}$$

where k is the penalty coefficient, Δx is the displacement between element N_i and the outer surface. The direction of P_c points to the normal direction of the outer surface.

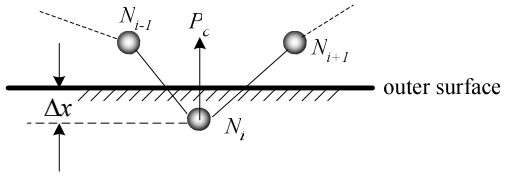

Fig. 15. the penalty method.

3.4 Force Feedback in Suturing

When the suturing begins, the mass element at the tail of the suture (element N_{n-1} in Fig. 16) and the element which is closest to the position to be sutured (element N_i in Fig. 16) are constrained by the tissue. The mass element at the head of the suture (element N_0 in Fig. 16) is constrained by the needle. The whole suture is pulled tensely and force F is fed back to the operator. When the time taken for the propagation of the force from mass element N_0 to mass element N_{n-1} is ignored, Eqn.(9) can be obtained,

$$F = k_i \cdot \Delta l_i \ (i=1,\ldots,n-1) \tag{9}$$

where F is the feedback force, k_i is the stiffness coefficient of the connecting spring S_i, and Δl_i is the elongation of S_i. The overall elongation of the suture Δl is calculated in Eqn.(10),

$$\Delta l = \sum_{i=1}^{n-1} \Delta l_i \tag{10}$$

So F can be calculated in Eqn. (11),

$$F = \frac{c \cdot \Delta l}{\sum_{i=1}^{n-1} \frac{1}{k_i}} \tag{11}$$

where c is a constant to map the value of F to the range within a range between *0* to *10* Newton which is applicable to the haptic device PHANToM® used in this research.

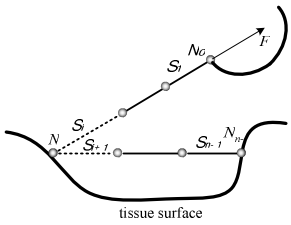

Fig. 16. Force feedback.

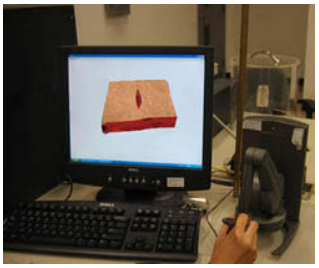

Fig. 17. The overall system.

3.5 Implementations

The simulation is implemented on a PHANToM® device. Software used includes VC++, OPENGL for graphic rendering and GHOST® API for haptic rendering. Fig. 17 illustrates the overall system. Fig. 18 demonstrates the basic interactions with deformable tissue in real time. Fig. 18 (a), Fig. 18 (b), and Fig. 18 (c) illustrate the process how the wound is sutured. Fig. 19 shows the force feedback during different stage of the suturing process. The bar on the left is a real-time display of the force applied to the user through the Phantom device. The height of the black bar illustrates the magnitude of the force feedback. The haptic feeling together with the real-time force magnitude display allows the user to have a better assessment of the suturing process.

(a) (b) (c)

Fig. 18. The process of suturing. (a) Wound before suturing. (b) Wound being sutured. (c) Suturing finished.

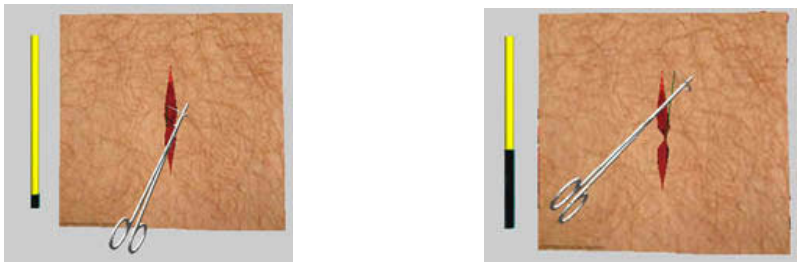

(a) A smaller force is felt in suturing (b) a larger force is felt in suturing

Fig. 19. The force feedback during the suturing process.

4. ACKNOWLEDGEMENT
This research is supported by a grant from Hong Kong Research Grants Council under the code HKU 7116/05E.

5. REFERENCES

[1] Basdogan, C., Ho, C. H. and Srinivasan, M. A., Virtual environments in medical training: Graphical and haptic simulation of laparoscopic common bile duct exploration, *IEEE/ASME Transactions on Mechatronics*, Vol. 6, No. 3, 2001, pp 269–285.
[2] Bourguignon, D. and Cani, M-P., Controlling Anisotropy in Mass-Spring Systems, Computer Animation and Simulation 2000, pp 113-123, Interlaken 2000.
[3] Bruyns, C. and Montgomery, K., Generalized Interactions Using Virtual Tools Within the Spring Framework: Cutting, Medicine Meets Virtual Reality (MMVR02), Newport Beach, CA, January 23-26, 2001.
[4] Laugier, C., Mendoza, C. and Sundaraj, K., Towards a Realistic Medical Simulator using Virtual Environments and Haptic Interaction. In Proc. of the International Symposium in Reserach Robotics, Sidney (AU), 2001.
[5] Bielser, D. and Gross, M. H., Interactive Simulation of Surgical Cuts. Pacific Graphics 2000. October 03 - 05, 2000. Hong Kong, China
[6] Hutchinson, D., Preston, M., and Hewitt, T., Adaptive refinement for mass/spring simulation. In 7th Eurographics Workshop on Animation and Simulation, pp. 31-45, Poitiers, France, September 1996
[7] Weiss, D. J. and Okamura, A. M., Haptic Rendering of Tissue Cutting with Scissors. 12th Annual Medicine Meets Virtual Reality Conference, January, 2004, Newport Beach, CA
[8] Chen, D. T. and Zeltzer, D., Pump It Up: Computer Animation of a Biomechanically Based Model of Muscle Using the Finite Element Method, *Computer Graphics*, Vol. 26, No. 2, 1992, pp 89-98.
[9] van den Bergen, G., Efficient Collision Detection of Complex Deformable Models Using AABB Trees, *Journal of Graphics Tools*, Vol. 2, No. 4, 1999, pp 1-14.
[10] Berkley, J., Turkiyyah, G., Berg, D., Ganter, M. and Weghorst, S., Real-Time Finite Element Modeling for Surgery Simulation: An Application to Virtual Suturing, *IEEE Transactions on Visualization and Computer Graphics*, Vol. 10, No. 3, 2004.
[11] Brown, J., Montgomery, K., Latombe, J.-C., Michael Stephanides, M., A Microsurgery Simulation System. MICCAI, 2001, pp 137-144.
[12] Kim, J., De, S. and Srinivasan, M. A., computationally efficient techniques for real time surgical simulation with force feedback. Proc. of IEEE VR2002 Conference, Orlando, Florida, March, 2002.
[13] Kühnapfel, U. Çakmak, H. K., Maass, H., Endoscopic surgery training using virtual reality and deformable tissue simulation. *Computers & Graphics*, Vol. 24, 2000, pp 671-682.
[14] Lin, M. and Gottschalk, S., Collision detection between geometric models: a survey. In: Proc. of the IMA Conf. on Mathematics of Surfaces. 1998, pp. 37-56.
[15] Maurel, W., Wu, Y., Magnenat Thalmann, N. and Thalmann, D., Biomechanical Models for Soft Tissue Simulation, Springer-Verlag, Berlin/Heidelberg, 1998, pp 17.
[16] Bro-Nielsen, M. and Cotin, S., Real-time Volumetric Deformable Models for Surgery Simulation using Finite Element and Condensation, EUROGRAPHICS'96, Vol. 15, No. 3, 1996, pp C-57-C-66.
[17] Bro-Nielsen, M., Finite Element Modeling in Surgery Simulation, *Journal of IEEE*, Vol. 86, 1998, pp 490-503.
[18] Nedel, L. P. and Thaimann, D. Real Time Muscle Deformations Using Mass-Spring Systems, Computer Graphics International 1998, 1998, pp. 156-165.
[19] Okamura, A., Simone, C., O'Leary, M., Force Modeling for Needle. Insertion into Soft Tissue, *IEEE Transactions on Biomedical. Engineering*, Vol. 51, No. 10, 2004.
[20] Picinbono, G., Lombardo, J.-C., Delingette, H., Ayache, N., Anisotropic elasticity and force extrapolation to improve realism of surgery simulation. Proc. ICRA 2000 (IEEE International Conference on Robotics and Automation, San Francisco, USA, 24-28 April 2000), 1, pp 596-602.
[21] DiMaio, S. P. and Salcudean, S. E., Needle insertion modeling and simulation, in Proc. IEEE Int. Conf. Robotics Automat., 2002, pp 2098–2105.
[22] Cotin, S., Delingette, H., Ayache, N., A hybrid elastic model for real-time cutting, deformations, and force feedback for surgery training and simulation, *The Visual Computer*, Vol. 16, No. 8, 2000, pp 437-452.
[23] www.ablesw.com
[24] http://medlib.med.utah.edu/kw/derm/pages/prex_23.htm
[25] http://moon.ouhsc.edu/dthompso/namics/pasfor.htm